

CONSTRAINING THE PROPERTIES OF DELTA SCUTI STARS USING SPECTROSCOPIC ECLIPSING BINARY SYSTEMS

O. L. CREEVEY^{1,2}, T. S. METCALFE³, T. M. BROWN⁴, S. JIMÉNEZ-REYES¹, AND J. A. BELMONTE^{1,2}

Draft version November 5, 2018

ABSTRACT

Many stars exhibit stellar pulsations, favoring them for asteroseismic analyses. Interpreting the oscillations requires some knowledge of the oscillation mode geometry (spherical degree, radial and azimuthal orders). The δ Scuti stars ($1.5 - 2.5 M_{\odot}$) often show just one or few pulsation frequencies. Although this may promise a successful seismological analysis, we may not know enough about either the mode or the star to use the oscillation frequency to improve the determination of the stellar model, or probe the star's structure. For the observed frequencies to be used successfully as seismic probes of these objects, we need to concentrate on stars for which we can reduce the number of free parameters in the problem, such as binary systems or open clusters. We investigate how much our understanding of a δ Scuti star is improved when it is in a detached eclipsing binary system instead of being a single field star. We use singular value decomposition to explore the precision we expect in stellar parameters (mass, age and chemical composition) for both cases. We examine how the parameter uncertainties propagate to the luminosity – effective temperature diagram and determine when the effort of obtaining a new measurement is justified. We show that for the single star, a correct identification of the oscillation mode is necessary to produce strong constraints on the stellar model properties, while for the binary system the observations without the pulsation mode provide the same or better constraints on the stellar parameters. In the latter case, the strong constraints provided by the binary system not only allow us to detect an incorrectly-identified oscillation mode, but we can also constrain the oscillation mode geometry by comparing the distribution of possible solutions with and without including the oscillation frequency as a constraint.

Subject headings: asteroseismology — binaries: eclipsing — stars: fundamental parameters — stars: variables: delta Scuti — methods: analytical — methods: numerical

1. INTRODUCTION

δ Scuti stars are a class of pulsating objects located on the Hertzsprung-Russell (H-R) diagram on and near the main sequence (MS) where it intersects the classical instability strip (see Breger 2000 for a review). They are $1.5 - 2.5 M_{\odot}$ stars often pulsating in one dominant oscillation mode or in many lower-amplitude modes. Originally they were thought to be very interesting targets for an asteroseismic analysis because 1) their pulsations are easily detected with ground-based telescopes, and 2) we understand the structure of MS stars relatively well (e.g. Metcalfe et al. 2009). Consequently, asteroseismology of these stars was thought to have the potential to probe the details of the interior, such as energy transport mechanisms and convective core overshoot, as well as less well-understood phenomena such as rapid rotation (Featherstone et al. 2007; MacGregor et al. 2007).

Unfortunately, successful asteroseismic analyses are infrequent for several reasons. 1) Observationally, the labeling of each measured frequency with its geometric characteristics (mode identification) is not trivial. For example, rapid rotation causes each of the mode

degrees ℓ to split into $(2\ell + 1)$ components with different azimuthal order (m) (Goupil et al. 2005). Also some of the stars are sufficiently evolved to show mixed modes (Metcalfe et al. 2010), thus complicating the analysis. 2) Theoretically, it is difficult to find a unique model to match the set of observed frequencies, even with additional observational constraints. With the fundamental stellar properties poorly constrained, use of the mode as a "seismic probe" is severely limited. For example, the multi-periodic δ Scuti star FG Vir, has been the target of many observational campaigns, allowing the detection of more than 75 frequencies (Breger et al. 2005), and the identification of 12 modes (Daszyńska-Daszkiewicz et al. 2005; Zima et al. 2006). Even with these observational constraints, the stellar parameters such as mass and helium mass fraction remain uncertain (Guzik & Bradley 1995; Viskum et al. 1998; Templeton et al. 2001; Kirbiyik et al. 2005). A similar case is XX Pyx (see Handler 2002 for a review). Handler (2002) noted that even searching among more than 40,000 models in a three-dimensional parameter space, Pamyatnykh et al. (1998) could not find a model that matched the observations.

The lack of successful asteroseismic analyses has encouraged authors to reconsider their approach. On the one hand, much progress has been made in observational mode identification, while on the other, authors are beginning to study these stars in systems where the number of free parameters is reduced (Lampens & Boffin 2000; Aerts & Harmanec 2004; Maceroni 2006; Costa et al. 2007). For ex-

Electronic address: orlagh@iac.es

¹ Instituto de Astrofísica de Canarias, C/ Vía Láctea s/n, E-38200 Tenerife, Spain.

² Universidad de La Laguna, Avda. Astrofísico Francisco Sánchez s/n, 38206 La Laguna, Tenerife, Spain.

³ High Altitude Observatory/National Center for Atmospheric Research, Boulder, Colorado 80301, USA

⁴ Las Cumbres Observatory Global Telescope Network Inc., 6740 Cortona Dr. Suite 102, Santa Barbara, CA 93117, USA.

ample, open clusters provide constraints on the age and metallicity (Fox Machado et al. 2006; Saesen et al. 2010), while multiple systems allow precise determinations of the mass and radius (Escolà-Sirisi et al. 2005; Hekker et al. 2010; Maceroni et al. 2010). The ideal pulsating star would be part of an eclipsing binary within an open cluster (Arentoft et al. 2007; Creevey et al. 2009; Stello et al. 2010; Talamantes et al. 2010).

Using asteroseismology to probe the interior of a star requires the global properties to be known quite well. For example, the mass should be known to 1-2%. Fortunately, the measurable quantities from a binary system can provide strong constraints on the properties of the component stars. If the binary is an eclipsing and double-lined spectroscopic system (SB2), the absolute values of the masses and radii can be determined with 1-2% precision e.g. Ribas et al. (1999); Lastennet et al. (2000).

Many new detached eclipsing binaries are being discovered by several satellites dedicated to photometric monitoring of stars (MOST Matthews 2004, CoRoT Baglin et al. 2002, *Kepler* Borucki et al. 2003), as well as numerous ground-based surveys (Henry 1998; Brown & Charbonneau 2000; Bakos et al. 2002; Pollacco et al. 2006). Some of these systems have components that exhibit stellar oscillations (Maceroni et al. 2010; Hekker et al. 2010). We will soon be faced with the problem of choosing which systems to study.

In this paper, we use singular value decomposition (SVD) to study the information content of stellar systems. This theoretical investigation quantifies the increase in astrophysical information realized by studying pulsating stars in detached eclipsing SB2 binaries (binary) instead of single pulsating field stars (single star), especially for those cases where mode identification is difficult. We assume that in a detached system, the stellar structure is unaltered by the binarity. The particular questions we address are:

- What is the role of each observable for a single star, and how do these roles change if the star is observed in a binary system?
- With the additional constraints for the binary system, how does the error box in the H-R diagram compare to that of a single star? If the mode geometry is successfully identified through observational methods, how does this error box change?
- Given the typical observational errors, what are the expected uncertainties in the model parameters for the single star and the binary system?
- Are the constraints on the stellar parameters sufficient to distinguish between possible solutions when a mode is incorrectly identified?

In Section 2 we introduce the definitions, models, observations and method necessary to understand the rest of this work. In Section 3 we study the roles that the observations play for determining the stellar model solution for both a single star and a binary stellar system, and we highlight which observations are most informative. In Section 4 we then discuss the parameter uncertainties, the error ellipses, and the error box in the

H-R diagram, which show more specifically which observations are capable or incapable of reducing these uncertainties. Finally in Section 5 we use simulations to show that an incorrectly-identified oscillation mode can be detected in the binary system, but not in the single star. We also show that the binary observations alone can constrain and even identify the mode geometry by studying the distribution of model solutions without observational constraints on the mode.

2. MODELS, OBSERVATIONS AND METHODS

Our method follows that of Brown et al. (1994) who used SVD as a diagnostic tool to investigate how useful oscillation frequencies are as constraints on stellar parameters in a visual binary system, using α Cen A as an example. This work was followed up in Creevey et al. (2006) and Creevey et al. (2007) and the techniques are also presented in Press et al. (1992) and Miglio & Montalbán (2005). We refer the reader to these papers for details on the method.

2.1. The distinction between parameters and observables

We define a *parameter* as an input characteristic to a stellar model, for example, mass and age. These are the quantities that we wish to determine. An *observable* is an output quantity from a stellar model given a set of parameters e.g. a radius, metallicity or a photometric magnitude V . We compare the theoretical observables to the real observations in order to retrieve the parameters. For example, we can measure the effective temperature of a star (observation) and its error, and use these to retrieve the mass and age (parameters) for a stellar evolution model by comparing the observed effective temperature to the theoretical/model effective temperature (observable).

2.2. Stellar parameters and models

We describe a single δ Scuti star by a set of parameters \mathbf{P} . These are mass M , age τ , rotation (we use rotational velocity v), initial hydrogen X (or helium Y) and heavy metal Z mass fraction where $X + Y + Z = 1$, and mixing-length parameter α , where applicable. Figure 1 shows the derivatives of the two most sensitive observables (the effective temperature and an oscillation mode) with respect to α for a range of stellar masses. For values above $1.7 M_{\odot}$, we can clearly see that the considered observables are insensitive to α , and can be ignored. The Aarhus STellar Evolution Code (ASTEC) (Christensen-Dalsgaard 2008) is used to calculate the stellar evolution models. The ASTEC code uses the equation of state of Eggleton et al. (1973), without Coulomb corrections, and the OPAL opacities (Iglsias & Rogers 1996), supplemented by Kurucz opacities at low temperatures. The nuclear reaction rates come from Bahcall & Pinsonneault (1992), convection is described by the mixing-length theory of Böhm-Vitense (1958), convective core overshooting is included with α_{ov} set to 0.3, and diffusion effects are ignored. This code uses the stellar parameters described above as the input ingredients and returns a set of global stellar properties such as radius R and effective temperature T_{eff} (observables), and the interior profiles of the stellar mass, density and pressure. Oscillation frequencies are calculated using MagRot (Gough & Thompson 1990;

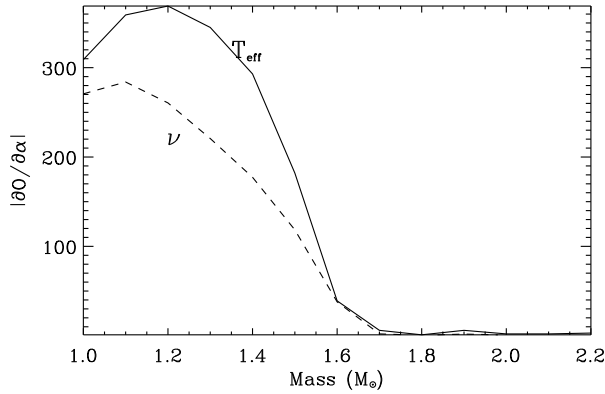


FIG. 1.— The dependence of the most sensitive observables (effective temperature and an oscillation mode) on the convective envelope mixing-length parameter for a range of stellar masses.

TABLE 1
SYSTEM PARAMETERS

Parameter	Value (P_j)	Parameter	Value (P_j)
M_A	1.80 M_\odot	v_A	100.0 km s $^{-1}$
M_B	1.70 M_\odot	v_B	60.0 km s $^{-1}$
X	0.700	Z	0.035
τ	0.700 Gyr	d	200 pc
a	0.150 AU	i	85.6°
e	0.0	γ	0.0 km s $^{-1}$
(ω)	(0.0)		

Burke & Thompson 2006). The distance d is also included as a stellar parameter, and coupling this with R , M , T_{eff} and the metallicity $[M/H]$, allows us to calculate magnitudes using model atmospheres (Lejeune et al. 1997).

For a binary system, the additional model parameters are the system properties: orbital semi-major axis a , orbital eccentricity e , longitude of periastron ω , systemic velocity γ , and orbital inclination i (note that i will always denote inclination unless otherwise specified). Both stellar components of a binary system share the parameters τ , X and Z , so the individual stars differ only in M and v . We shall use the subscripts 'A' and 'B' to denote the components of the binary. The parameters of the model system are given in Table 1, and while these are not based on any particular binary system, there are known systems whose masses approximate these, such as HD 172189, HD 26591, HD 42083. We also note that the system stars pursue non-synchronised rotation, compatible with our earlier assumption that the stars evolve "individually".

2.3. System observables and observations

The observables are the measurable quantities of the system. These include things such as R (from interferometry for example), T_{eff} , $[M/H]$, gravity $\log g$, and parallax π for a single star. For a binary system, additional observables include effective temperature ratio T_{BA} ($= T_B/T_A$), relative radii R_{BA} , semi-amplitudes of radial velocity curves K_A and K_B , and orbital period Π . We note that the radial velocity or light curve measurements are also considered observables, however, in this work the

more intuitive derived values (T_{BA} , $M_A \sin^3 i$, $M_B \sin^3 i$, ω etc.) are used.

Using model atmospheres (Lejeune et al. 1997) with d and R , we calculate the photometric magnitudes (r , i , and z) using the SDSS filter system (York et al. 2000). These atmospheres take reddening into account. We subsequently calculate the colors from these magnitudes, although we note that distance d is not necessary to obtain approximate color indices. The colors we include in our analysis are $(r - i)$ and $(i - z)$ and the magnitude is r . For the binary, the photometric observables are calculated from blended spectra. Two or more blended colors yield estimates of the individual and relative quantities of the component properties. The colors of the individual components can be disentangled (Koch 1960; Semeniuk 2001; Creevey et al. 2005). However, obtaining component colors with the same precision as the system can only be achieved with high quality multi-color light curves.

From the light curve of an eclipsing binary system we obtain R_{BA} , T_{BA} , i and Π . We use these derived values from the modeling of the binary system for simplicity and to understand the errors in terms of what is quoted in the literature. The derived observables are valid, as long as we correctly propagate the uncertainties from the light curve data.

Spectroscopy provides the observables $v_A \sin i$ and $v_B \sin i$ (projected rotational velocity) and the atmospheric parameters $\log g$, T_{eff} and $[M/H]$. An observed spectrum for a binary system is the sum of the spectra from the two stellar components. Many observational techniques exist to disentangle spectra e.g. Hadrava (1995, 2009), and these techniques have been successful, see Creevey et al. (2009) for a specific case using various techniques to determine the individual component T_{eff} for HD 172189. We assume that we can successfully disentangle the spectra and obtain effective temperatures for both stars while using the photometric T_{BA} as a constraint.

A time series of spectroscopic measurements yields a time series of radial velocities, and modeling these data yields $M_A \sin^3 i$, $M_B \sin^3 i$, $a \sin i$, e , ω and γ . Coupling these values with i and R_{BA} (from photometry) provides the absolute values of the radius.

A time series of radial velocity or photometric measurements provides the frequency(ies) ν of the modes that are excited in the star. However, the frequencies are only useful if we know the oscillation mode geometry (the degree ℓ , the azimuthal order m and the radial order n of the wave). This so-called "mode-identification" can be achieved by either studying the time series of spectroscopic line-profiles of the star (Kennelly et al. 1990; Horner et al. 1996; Balona 2000; Briquet & Aerts 2003; Zima 2006), by using multi-color photometry and comparing the oscillation amplitudes and the phases of the frequencies in various filter bands (Garrido 2000; Dupret et al. 2003; Daszynska-Daszakiewicz et al. 2007), or by using the screening effects of the eclipses in eclipsing binaries (Bíró & Nuspl 2005; Gamarova et al. 2005). Many δ Scuti pulsators have only one dominant oscillation frequency and so the assumption is that we measure at least one precise frequency.

The values of the errors (c.f. Table 2) are chosen by considering typical observations for such systems, but also

TABLE 2
OBSERVABLES AND ERRORS

Observable (B_i)	Error (ϵ_i)			
		Figs. 2,3,5	Figs. 4,8	Figs. 7-11
R_A (R_\odot)	1.95	0.02	0.01	0.04
R_B (R_\odot)	1.81	0.04	0.01	0.04
T_{BA}	0.97	0.05	0.05	0.05
i ($^\circ$)	85.6	1.0	1.0	0.3
$T_{\text{eff}A}$ (K)	6965	100	100	100
$v_A \sin i$ (km s^{-1})	99.7	2.5	2.5	2.5
$v_B \sin i$ (km s^{-1})	59.8	2.5	2.5	2.5
Π (yrs)	3.1053e-6	1e-6	1e-6	1e-6
$M_A \sin^3 i$ (M_\odot)	1.78	0.06	0.10	0.04
$M_B \sin^3 i$ (M_\odot)	1.69	0.05	0.10	0.03
$[M/H]$ (dex)	0.31	0.05	0.05	0.05
$\log g$ (dex)	4.1	0.5	0.5	0.5
π (mas)	5.0	0.5	0.5	0.5
r (mag)	8.16	0.02	0.02 [†]	0.01
$(r - i)$ (mag)	0.178	0.003	0.005 [†]	0.001
$(i - z)$ (mag)	0.009	0.003	0.005 [†]	0.001
ν (μHz)	1108.9	1.3	1.3 ^{††}	1.3

[†] 0.5 mag for Fig. 4 top panel. ^{††} 1e4 μHz for the black ellipse in Fig. 8

to study some limiting cases, for example when the errors reach the limits of current techniques, or if the stars are bright (closer in distance). We assume that the light curves cover a few orbital periods. Spectroscopic data, however, are more time-consuming and the demand for observation time is high, especially for larger telescopes. Thus, one may hope that spectroscopy during one full orbital period can be obtained, with some data points during subsequent orbits. Taking into account that one of the stars is pulsating, this will impact the analysis of both the photometric and spectroscopic data. In particular the depths of the eclipses will need to be observed several times to remove the effects of the modulations due to pulsation, and this influences the derivation of T_{BA} , R_{BA} , and Π , for example. Spectroscopy will show clear line-profile variations, and deviations in the expected radial velocities due to pulsation. Both of these will influence the determination of the orbital radial velocities to some extent, and these will in turn affect the errors in M , R and Π . Table 2, first column, lists the values of the observables calculated from the stellar model defined by the parameters in Table 1. The subsequent columns show the corresponding errors used for this analysis. We have considered errors (ϵ) in mass-related and radius observables of the order of 1-3%. The 3% error should account for the effects of pulsation on the data. Errors of 100 K, 0.05 dex and $0.3 - 1.0^\circ$ for T_{eff} , T_{BA} , and i are values typically found in the recent literature (Ribas et al. 2002; Southworth et al. 2004; Hilditch et al. 2005; Sousa et al. 2006; Bruntt et al. 2010). We use 2.5 km s^{-1} as the error on the projected rotational velocity (e.g. Creevey et al. 2009). Reducing the precision on these values influences the determination of the rotational velocity of the star. Unfortunately including rapid rotation is a complex matter for stellar models, and most stellar codes (including those used in this work) consider only solid-body rotation which has minimal effect on the non-seismic observables.

TABLE 3
OBSERVABLE (OS) AND PARAMETER (P) SETS USED IN THIS ANALYSIS. AS DENOTES ADDITIONAL OBSERVABLES AND THE SUBSCRIPTS 'S' AND 'EB' REFER TO SINGLE STAR AND ECLIPSING BINARY SYSTEM.

OS_S =	$\{R, T_{\text{eff}}, \log g, v \sin i, [M/H], \pi\}$
OS_{EB} =	$\{R_A, R_B, T_{BA}, i, T_{\text{eff}A}, v_A \sin i, v_B \sin i, \Pi, M_A \sin^3 i, M_B \sin^3 i, [M/H], \pi\}$
AS1 =	$\{\nu\}$
AS2 =	$\{r, r - i, i - z\}$
AS3 =	$\{r, r - i, i - z, \nu\}$
P_S =	$\{M, \tau, X, Z, v, i, d\}$
P_{EB} =	$\{M_A, M_B, \tau, X, Z, v_A, v_B, i, d, [a, e, \omega, \gamma]\}$

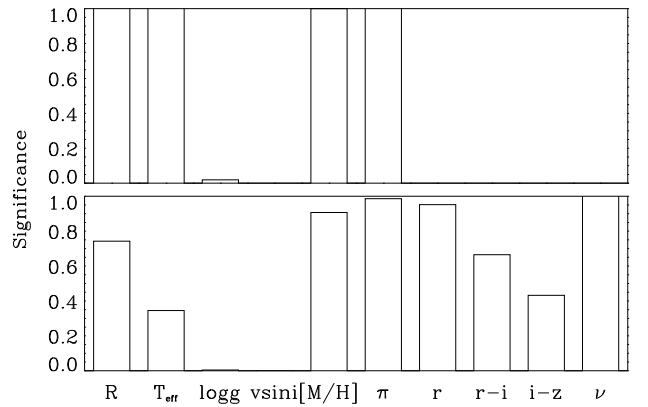


FIG. 2.— Significance of observables sets without colors, magnitudes and the oscillation mode (**OS_S** — top) and including these data (**OS_S+AS3** — bottom) for a single star.

The precision in the photometric values is typical for well-determined literature values. We chose some limiting values ($\epsilon < 0.003$) because at these precisions the colors begin to have an important impact for the determination of the parameters. The frequency error of 1.3 μHz corresponds to the frequency resolution of data from a one-week observational campaign. We increase the values of these errors for some calculations (note in Table 2) to eliminate their influence.

An analysis of the influence that each observation has (see next section) for different sets and errors, and an investigation of the parameter uncertainties led us to choose four competitive sets of observables to study, and these are given in the top part of Table 3. **OS** is the base *observable set* used, and **AS1**, **AS2** and **AS3** are the *additional sets*. The subscripts 'S' and 'EB' denote 'single star' and 'eclipsing binary' respectively. For the remainder of this work we discuss our results in terms of each of these sets and we remove the bold text: OS, OS+AS1, OS+AS2 and OS+AS3. We include the subscripts 'A' and 'B' on the observables and parameters to denote each component in the binary system when necessary, and the magnitudes and colors also have a subscript 'EB' to emphasize that these are binary system (blended) observables.

We do not include $a \sin i$ as an observable because it

does not provide independent information. We can calculate it from three of the following: $M_A \sin^3 i$, $M_B \sin^3 i$, $q \equiv K_A/K_B = M_B/M_A$, and Π using Kepler's Third Law.

2.4. Singular value decomposition method

SVD is the decomposition of any $M \times N$ matrix \mathbf{D} into 3 components: \mathbf{U} , \mathbf{V} and \mathbf{W} given by $\mathbf{D} = \mathbf{U}\mathbf{W}\mathbf{V}^T$. \mathbf{V}^T is the transpose of \mathbf{V} which is an $N \times N$ orthogonal matrix that contains the *input* basis vectors for \mathbf{D} or the vectors associated with the parameter space. \mathbf{U} is an $M \times N$ orthogonal matrix that contains the *output* basis vectors for \mathbf{D} , or the vectors associated with the observable space. \mathbf{W} is a diagonal matrix that contains the *singular values* of \mathbf{D} .

The key element to this work is the description of the matrix \mathbf{D} , which we call the design matrix and each element is a partial derivative of each of the observable with respect to each of the parameters of the system, taking into account the measurement errors for each of the observables:

$$D_{kj} = \frac{\partial B_k}{\partial P_j} / \epsilon_k. \quad (1)$$

Here B_k are each of the $k = 1, 2, \dots, M$ observables of the system with expected errors ϵ_k , and P_j are each of the $j = 1, 2, \dots, N$ free parameters of the system (see section 2.2 for discussion on the observables and the parameters).

By writing the design matrix with the measurement errors taken into account, we provide a quantitative description of the information content of each of the observables for determining the stellar parameters and their uncertainties.

Starting from an initial close guess of the solution \mathbf{P}_0 , SVD can be used as an inversion technique to obtain the true solution \mathbf{P}_R of the system. This is done by calculating a set of parameter corrections $\delta\mathbf{P}$ that minimizes some goodness-of-fit function: $\delta\mathbf{P} = \mathbf{V}\bar{\mathbf{W}}^{-1}\mathbf{U}^T\delta\mathbf{B}$, where $\delta\mathbf{B}$ are the differences between the set of actual observations \mathbf{O} and the calculated observables \mathbf{B}_0 given the initial parameters \mathbf{P}_0 . $\bar{\mathbf{W}}$ is a modification of the matrix \mathbf{W} such that the inverses of all values below a certain threshold are set to 0. The formal errors comprise the sum of all of the \mathbf{V}_q/w_q , where each \mathbf{V}_q/w_q describes the direction and magnitude to change a parameter so that the true solution \mathbf{P}_R and formal uncertainties can be given by

$$\mathbf{P}_R = \mathbf{P}_0 + \mathbf{V}\bar{\mathbf{W}}^{-1}\mathbf{U}^T\delta\mathbf{B} \left(\pm \frac{\mathbf{V}_1}{w_1} \pm \frac{\mathbf{V}_2}{w_2} \pm \dots \pm \frac{\mathbf{V}_N}{w_N} \right). \quad (2)$$

The *covariance matrix* \mathbf{C} consequently assumes a neat and compact form:

$$C_{jl} = \sum_{q=1}^N \frac{V_{jq}V_{lq}}{w_q^2}, \quad (3)$$

and the square roots of the diagonal elements of the covariance matrix are the theoretical parameter uncertainties. Note that ϵ is reserved for *observational error* and σ for *parameter uncertainty*:

$$\sigma_j^2 = \sum_{q=1}^N \left(\frac{V_{jq}}{w_q} \right)^2. \quad (4)$$

Another useful property of SVD is the *significance* S of an observable. This can be quantified as a measure of the extent that a $1-\epsilon$ change in B_k shifts the inferred parameters towards the $1-\sigma$ error ellipsoid in parameter space. In this way, S quantifies the impact that an observable has for the determination of the parameter solution:

$$S_k = \left(\sum_{q=1}^N U_{kq}^2 \right)^{1/2}. \quad (5)$$

Because of the orthonormality of the decomposition matrices, the value of S varies between 0 and 1. A low S_k implies that the observable B_k has relatively less influence on the solution, and that a change in the measurement will have little or no impact. A high value of S_k implies that this observable is important for the solution and any change in the measurement will force a corresponding change in the solution.

Finally, the matrices \mathbf{U} and \mathbf{V} provide information about the role each of the observables plays in determining the stellar parameters. Each column vector of \mathbf{U} (U_j) is related uniquely to each column vector of \mathbf{V} (V_j) and its importance in the solution is given by the corresponding singular value w_j (cf. Fig 4). In section 3.1.2 we elaborate on this discussion.

3. BINARY SYSTEM VERSUS SINGLE STAR CONSTRAINTS

In this section we investigate the roles that each observable plays for determining each parameter. We study how these roles change when we include/exclude certain observables and when we consider different values of the observational errors.

3.1. Single star observables

3.1.1. Significance

Figure 2 shows the significance (Eq. 5) of each of the observables for a single star for OS_S (top panel) and $\text{OS}_S+\text{AS3}$ (lower panel), using the measurement errors from the second column in Table 2. Because there is no information about i (inclination), the figure illustrates that $v \sin i$ is not an effective constraint ($S = 0$). Although, the value of $v \sin i$ imposes a lower limit on v , we can not determine its uncertainty. $\log g$ is also a weak constraint, because both R and T_{eff} provide similar information, but of better quality. If either of these were not available, then $\log g$ would have a higher significance. $S = 1$ implies that R , T_{eff} , $[\text{M}/\text{H}]$, and π are all necessary observations to constrain \mathbf{P}_S . By including the photometric information and the mode (lower panel), the most noticeable change is the reduction in $S(T_{\text{eff}})$, whose information is superseded mainly by r and $(r-i)$. $S(\nu) = 1$ indicates that the mode has a strong influence on the determination of the solution.

Figure 3 shows how S changes for each observable as some measurement errors are varied. The left panel shows $S(r-i)$, $S(R)$ and $S(T_{\text{eff}})$ as ϵ_{r-i} is varied for $\text{OS}_S+\text{AS2}$. Similar results are found for $\text{OS}_S+\text{AS3}$. $S(r-i)$ decreases as its error increases to values of about 0.004 mag, and, at this value, $S(R)$ begins to supersede $S(r-i)$. $S(T_{\text{eff}})$ also increases as the color measurement is more poorly determined, although it never increases to more than 0.45. The largest increase (or change) is seen only as ϵ_{r-i} reaches mmag precisions.

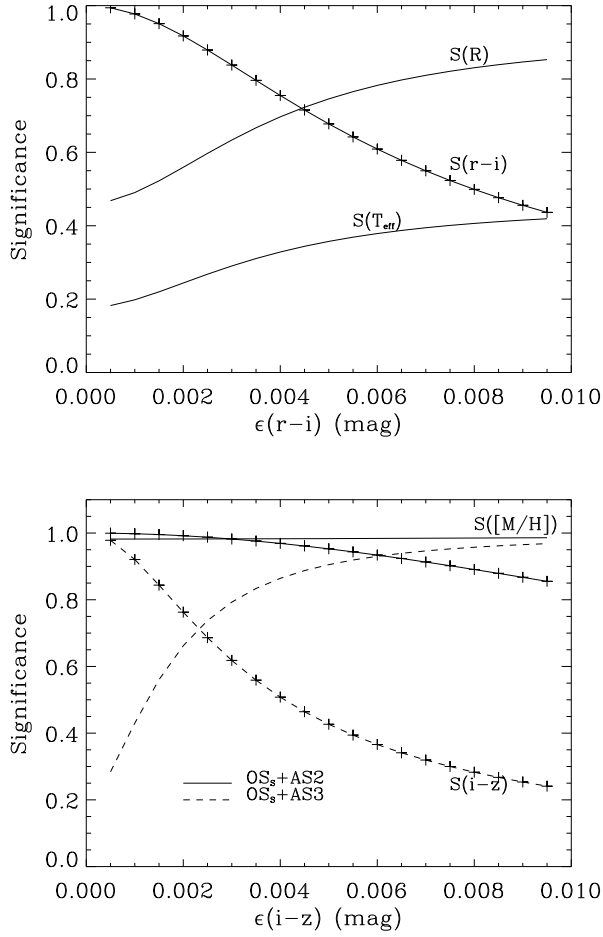


FIG. 3.— Change in observable significance S as the precision in photometric information changes for a single star. The photometric observables are denoted by crosses on their lines. *Left*: Similar results are found for sets OS_S+AS2 and OS_S+AS3, as the precision is decreased in ϵ_{r-i} . *Right*: Continuous and dashed lines denote OS_S+AS2 and OS_S+AS3, respectively, as the precision in ϵ_{i-z} is decreased.

The right panel of Figure 3 shows the change in $S([M/H])$ and $S(i-z)$ as ϵ_{i-z} increases in value. In this case, no other observable is affected. $(i-z)$ has a strong influence for determining the parameter solution only at precisions of ≤ 0.002 mag; for $(r-i)$ the critical value is ~ 0.004 mag (left panel). The difference between the continuous and the dashed lines is the inclusion of seismic data (AS3, dashed). Without seismic data, both $[M/H]$ and $(i-z)$ are important observables, while including seismic data, $[M/H]$ has little impact when $(i-z)$ is important, and vice versa. It is primarily the parameter Z that these observables are responsible for determining.

3.1.2. Transformation matrices

The decomposition matrices of SVD show which observables determine each of the parameters of the system. These are sets of linear vectors where each vector in \mathbf{U} is related uniquely to each vector in \mathbf{V} , and the relative importance of each vector is given by the corresponding singular value w_j in \mathbf{W} . In Figure 4, we show the transpose of these decomposition matrices for the single

star system, with the singular values represented in the right-most figure of both panels. These figures take into account the errors given in the third column of Table 2, except for the upper panel where the values for the colors have been increased to 0.5 mag and the frequency error to $1e4 \mu\text{Hz}$ to eliminate their influences.

In Figure 4 top panel, R , T_{eff} , and $[M/H]$ appear in the top three observable vectors indicating their importance for determining the combination of parameters, shown in vectors V_1 , V_2 and V_3 (mass, age, chemical composition). The next important observable (in U_6 — here $w_6 > w_4$) is π , and this is uniquely responsible for determining the distance (in V_6). Likewise, only the observable $v \sin i$ determines v , but poorly, and finally the observable with least information is $\log g$ (U_3 with smallest w_3), which contributes weakly to determining mass, age and chemical composition.

In the bottom panel of Figure 4, we have improved the errors in the photometric observables and the oscillation mode (third column in Table 2). These new observables now play a dominant role for determining the parameters, as can be seen from their positions in the top vectors, as well as an increase by a factor of 10 in the top singular values. Mass, age and chemical composition are much better constrained, mostly appearing in the top two panels. The contributions from T_{eff} and $\log g$ have diminished considerably, and the distance is now no longer determined uniquely by π . It also depends weakly on the photometric colors and magnitude (V_5 and U_5). As in the top panel, $v \sin i$ is responsible for determining v (U_6 and V_6). By omitting the oscillation frequency from the set of observables, R becomes the observable mostly responsible for determining M .

3.2. Binary system observables: Significance

The top panel of Figure 5 illustrates \mathbf{S} for OS_{EB} (binary system) using the errors from the second column of Table 2. This figure shows that the most important quantities are R_A , R_B , $T_{\text{eff}A}$, Π , $[M/H]$, $M_A \sin^3 i$, $M_B \sin^3 i$ and π . The lower panel shows \mathbf{S} for OS_{EB}+AS3. Note how each of the S values changes: including the magnitude, colors and oscillation frequency reduces the importance of R_A , $T_{\text{eff}A}$, $[M/H]$ and T_{BA} , while ever so slightly reducing $S(\pi)$. We note that i appears deficient in information content. An accurate and precise determination of i is necessary to correctly scale the observed values of $M_A \sin^3 i$ and $M_B \sin^3 i$. In this case $\epsilon(i) = 1.0^\circ$, however, increasing its precision to $< 0.3^\circ$ causes $S(i)$ to increase rapidly.

Figure 6 left panel shows $S(T_{\text{eff}A})$ and $S(r-i)_{EB}$ as ϵ_{r-iEB} changes for OS_{EB}+AS3. As ϵ_{r-iEB} decreases in precision, $S(r-i)_{EB}$ decreases from 1.0 to 0.6, while an increase in $S(T_{\text{eff}A})$ from 0.6 to 0.8 is also seen, perhaps implying that $(r-i)_{EB}$ is a temperature indicator. This is similar to the single star case but in the binary system $T_{\text{eff}A}$ remains relatively more important because the blended $(r-i)_{EB}$ provides less information (see Fig. 3 left diagram).

The right half of Figure 6 shows $S(R_A)$ as its precision is decreased for OS_{EB} and OS_{EB}+AS1. In the latter case, including an identified mode causes $S(R_A)$ to rapidly decrease in value, as it becomes more poorly determined. For some observables (T_{BA} , $M_{A,B} \sin^3 i$) S increases slightly during this change. At more than about

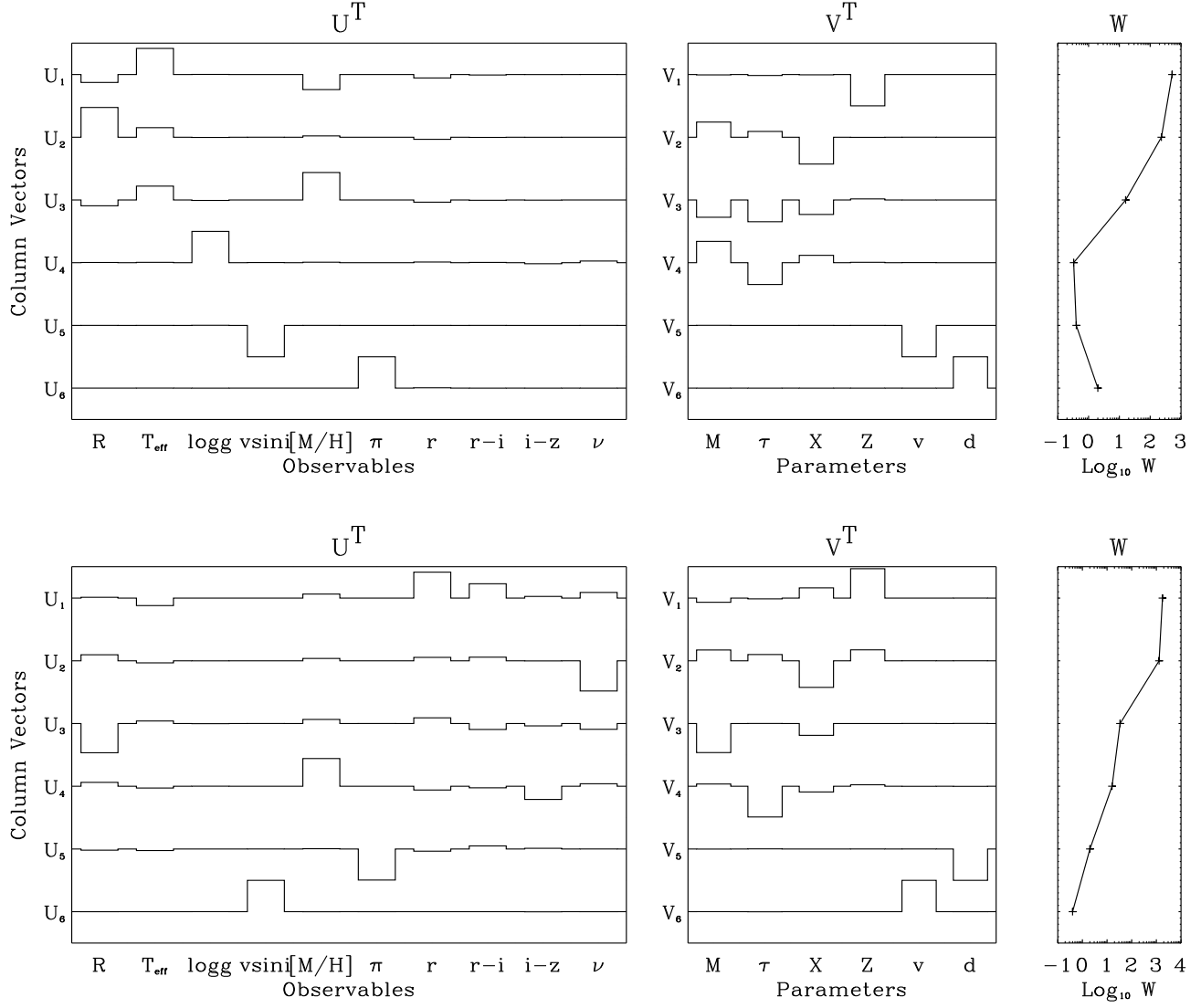


FIG. 4.— Decomposition matrices of a single star model using the errors given in Table 2, third column. The left, center and right panels are the matrices U^T , V^T and W respectively. The difference between the panels is the addition of well-constrained photometric and seismic data in the lower panels. These values are set to 0.5 mag and $1e4 \mu\text{Hz}$ respectively in the upper panel.

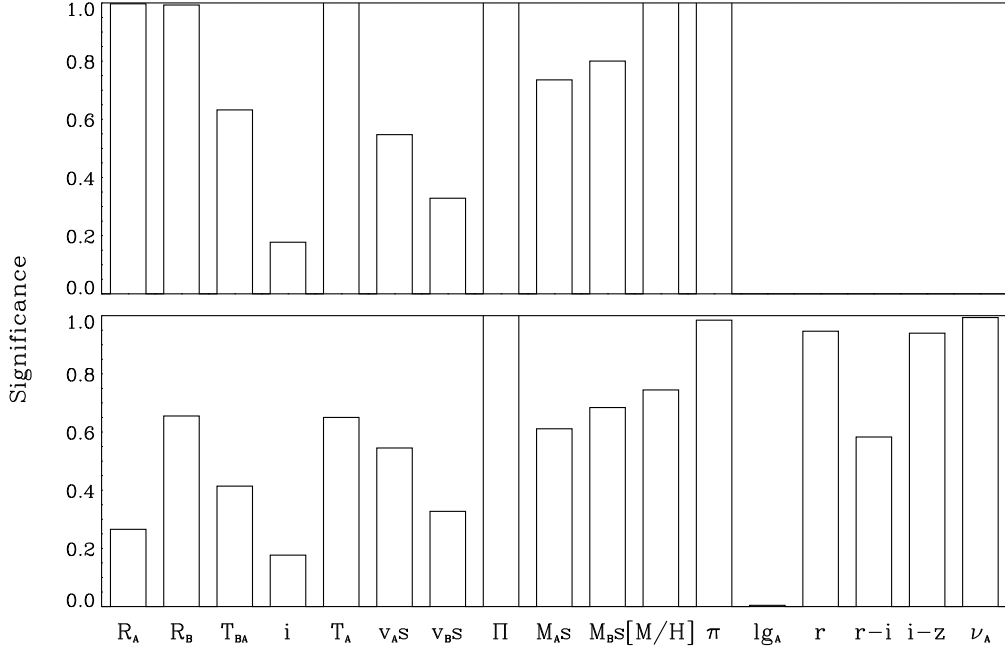


FIG. 5.— Significance of observables sets without/with photometric and seismic data (OS_{EB}/OS_{EB+AS3}) in top/bottom panels for a δ Scuti star in a detached eclipsing binary system. Note that we use an abbreviated labeling for the observables due to space constraints. The errors are given in the second column of Table 2.

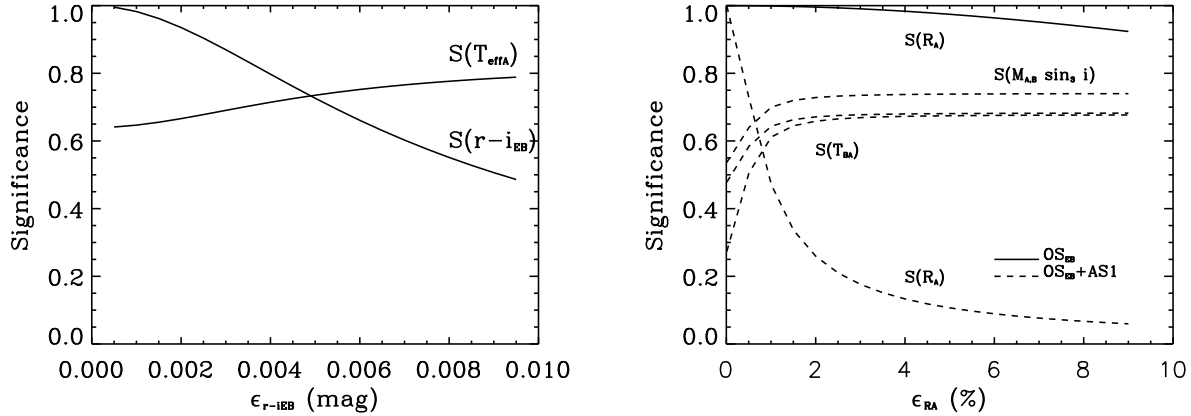


FIG. 6.— The relative significance of some binary observables as the precision in their errors changes. Left: $S(r-i)_{EB}$ and $S(T_{\text{eff}A})$ change as the precision in the system’s color ϵ_{r-iEB} decreases for OS_{EB+AS3} . Right: Change in S as ϵ_{RA} decreases in precision for OS_{EB} and OS_{EB+AS1} .

2% error, R_A has little role to play. On the other hand, for OS_{EB} , R_A remains relatively important at all considered errors, simply because there is no other observable in OS_{EB} that provides the same type of information.

4. DETERMINATION OF THE FUNDAMENTAL PARAMETERS OF THE PULSATING STAR

The observables that showed most sensitivity to a change in their precisions for different sets for either a single star or a binary system are R , T_{eff} , the photometric colors and an identified mode. In this section we study the uncertainties (Eq. 4) in the global parameters of the (primary) pulsating star as these observables are

improved/included for both a single star and a binary system.

4.1. Parameter uncertainties

To successfully use a single identified mode as a “seismic probe”, we need to know the fundamental stellar parameters M , τ , X , Z and v of the pulsating star with good precision. Here we discuss only the uncertainties in the first four, because the determination of v is independent of the determination of the others (the covariance off-diagonal elements ~ 0) and independent of most of the observable errors, except i and $v_A \sin i$. All of the other parameters of the system ($M_B \sin^3 i$, e , etc.) are

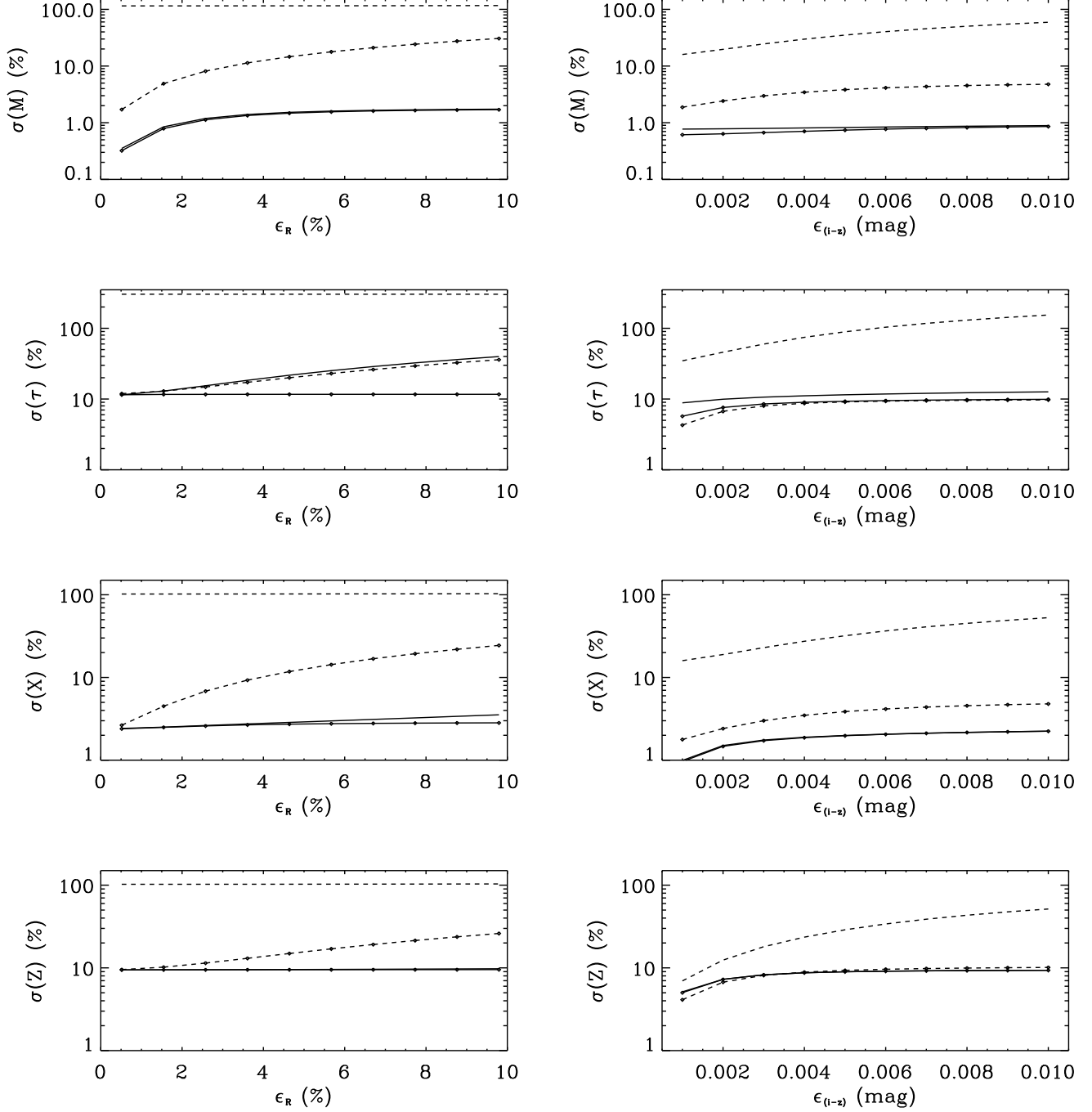


FIG. 7.— Theoretical uncertainties in the stellar parameters as the precision in ϵ_R (left) and ϵ_{i-z} (right) increases, for a single star (dashed lines) and a binary system (solid lines). The lines with dots represent the sets of observables with seismic information. The left panel shows the results without photometric constraints. The y-axis for each parameter has the same scale for comparing panels.

included for deriving the uncertainties, due to correlations that must be accounted for. However, we do not discuss these uncertainties because we are only interested in describing the pulsating star. As we are dealing with the primary (A) pulsating star only, we drop the subscript 'A' on all of the quantities.

Figure 7 shows the theoretical uncertainties in M (top), τ (second), X (third) and Z (lower panels) as we increase the precision in R (left panels) and both of the

photometric colors (right panels). The latter is denoted by ϵ_{i-z} and for the binary it implies the blended system's colors. The dashed and solid lines represent the single and binary system respectively, and the observable set with the identified mode has dots overplotted on the lines. The results for OS (both OS_S and OS_{EB}) and OS+AS1 are represented on the left panels, and those for OS+AS2 and OS+AS3 (including photometric information) on the right. Both the left and right panels show

the same y-axes scales for comparison.

It is very clear that the oscillation mode plays a very different role in the single star and the binary system. Excluding it from the single star constraints, without photometry, yields uncertainties $> 100\%$ and independent of ϵ_R ; the constraints are inadequate to determine the stellar model. Including the color constraints also yields large uncertainties ($> 30\%$) although not entirely independent of ϵ_{i-z} . When the mode is included, the uncertainties improve rapidly as the errors in both types of observables improve. In fact, $\sigma(M)$ becomes strictly dependent on ϵ_R as the error in the radius improves to $< 2 - 3\%$.

There is little difference seen in the parameter uncertainties for the binary system when the oscillation mode is included/excluded as a constraint. The binary system without any seismic data provides similar or better constraints on all of the parameters than the single star *with* an identified mode, except in some exceptional cases (see below). The fact that including a mode with the binary system constraints does not lead to improvements in the pulsating star's parameter uncertainties indicates that the binary constraints alone may provide sufficient constraints on the model to *use* the identified mode in a different way.

For the binary system, we also tested the effect of improving the precision in $M_A \sin^3 i$ and $M_B \sin^3 i$. Setting both of these values to 0.01, 0.05, and 0.10 M_\odot (0.5%, 2% and 5%) has little effect: for $\epsilon_R = 2\%$, $\sigma(M) = 0.3, 1.0$, and 1.5% respectively with and without the identified mode, and for $\epsilon_R > 4\%$, $\sigma(M)$ levels out to 0.3, 1.5, and 2.5%.

We note that for both $\sigma(Z)$ and $\sigma(\tau)$ for OS+AS3, in some cases the single star provides slightly better constraints than the binary. This happens only for very precisely measured (unblended) colors, while including an oscillation mode as a constraint. Finally, one should also note that $\sigma(X) \gtrsim 10\%$ is not a good constraint. The absolute value of the parameter is 0.700, and a 0.070 error on this value produces no meaningful constraint on X .

4.2. Parameter correlations

The \mathbf{V} matrix from the SV decomposition describes the correlations among the parameters, while the singular values scale each of the vectors V_j to produce the n-dimensional error ellipse axes. In Figure 8 we show projected contours of the 1- σ error box for τ versus M , and Z versus τ using the vectors that yield the largest ellipses. The black/grey ellipses correspond to the sets of errors in the third column of Table 2 for OS_{EB}+AS2/AS3. Including the oscillation mode does not reduce the error ellipse, and this reinforces the possibility of using this extra information to learn something else about the star.

4.3. H-R error box

Using equation (2) we calculate the theoretical uncertainties in the model effective temperature and model luminosity. Figure 9 shows the approximate theoretical error boxes for these quantities for a single star (OS_S+AS1, dashed lines) and a binary system (OS_{EB} solid lines). For the single star an identified mode is included because Fig. 7 and Sect. 4.1 showed that the parameters are not

constrained if the identified mode is not included, while for the binary system no seismic data are included.

The error box shrinks significantly in the luminosity axis while reducing the error in the radius for the single star (left panel). $\sigma(L_\star)$ also changes slightly with $\epsilon_{T_{\text{eff}}}$ (right panel), but its value is determined primarily by the error in the radius (2%). The left panel shows that interpolating between 1% and 3% for ϵ_R produces a $\sigma(L_\star) = 0.5 L_\odot$ for $\epsilon_R = 2\%$, as shown in the right panel.

As expected, the error box shrinks in the model effective temperature axis due to the reduced errors in the observational T_{eff} (right panel). The observational $\epsilon_{T_{\text{eff}}}$ of 200, 100, and 50 K produce model uncertainties $\sigma(T_{\text{eff}})$ of 250, 110, and 50 K. We do not expect these values to be reproduced exactly because the observed T_{eff} has a measurement error associated with it, and for large values of the error ($\sim 200\text{K}$), other observables can dominate the determination of the derived model parameter of T_{eff} . However, the fact that these uncertainties are approximately reproduced provides evidence that the SVD method is valid.

No identified mode is included with the binary system constraints (solid lines). The error box for the binary system does not shrink while reducing the errors in the radius (left panel). However, it shrinks when the error in the observed effective temperature is reduced, reproducing accurately the observational $\epsilon_{T_{\text{eff}}}$ of $\sigma(T_{\text{eff}}) = 200$, 100, and 50 K. $\sigma(L_\star)$ does not decrease in either panel, because the mass is well-determined for the binary system and provides this strong constraint on L_\star .

In all cases the constraints provided by the binary system without an identified mode on the parameters of the pulsating star are more effective than those from the single star when an identified mode is included.

5. INCORRECT MODE IDENTIFICATION

Asteroseismology is only useful when the observed frequencies have been correctly identified with their mode geometry. Although techniques exist to do this, is there a way to test if this identification is correct? In this section we show that an incorrectly identified mode can be diagnosed if the pulsating star is in the binary system, but not as a single star. We subsequently show that we can in fact constrain and/or identify the mode correctly by studying the distribution of model solutions.

We have shown that the oscillation mode is an important observation to have (Sect. 3) but including it as a constraint for the binary system did not improve the pulsating star's parameter uncertainties nor shrink the error box in the H-R diagram (Sect. 4). This implied that the mode is somewhat redundant information for defining the global quantities, and we concluded that the observed oscillation frequency could possibly be used in a different way. The oscillation mode occupies the top rows of the \mathbf{U}^T matrix in the single star (Fig. 4) and in the binary case, indicating that it is an observable that tightly constrains the stellar model. If the mode were incorrectly labeled, it should have a significant impact on the stellar parameter solution. We have also shown that the observational constraints from the binary system yield very well-determined parameters without using the oscillation mode (Figs. 7, 8). Therefore, we can compare the model solutions when we use a set of observables with and without the oscillation mode as a constraint.

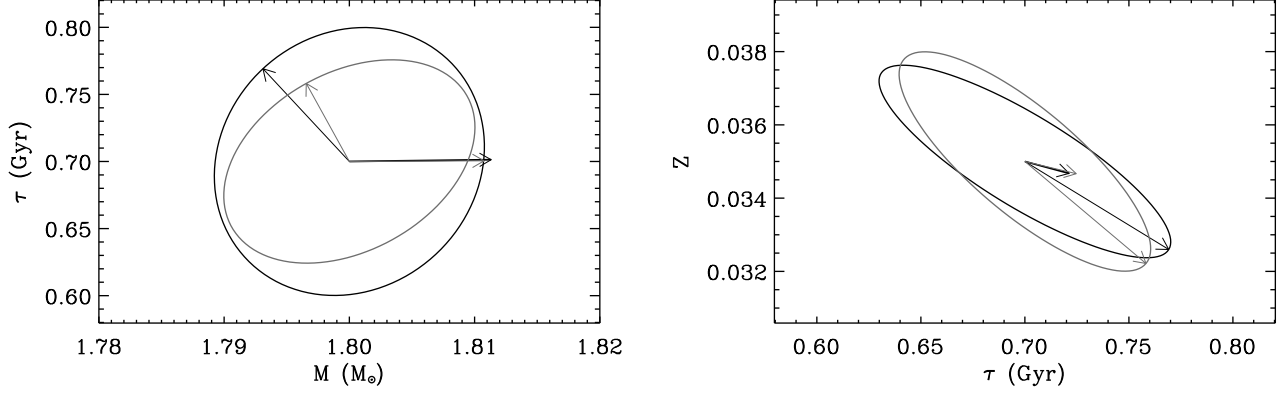


FIG. 8.— Maximum projections of the two-dimensional error ellipses defining the region of parameter space where the solution lies for the binary system, using $OS_{EB}+AS2$ (black) and $OS_{EB}+AS3$ (grey), and the observational errors given in the third column of Table 2.

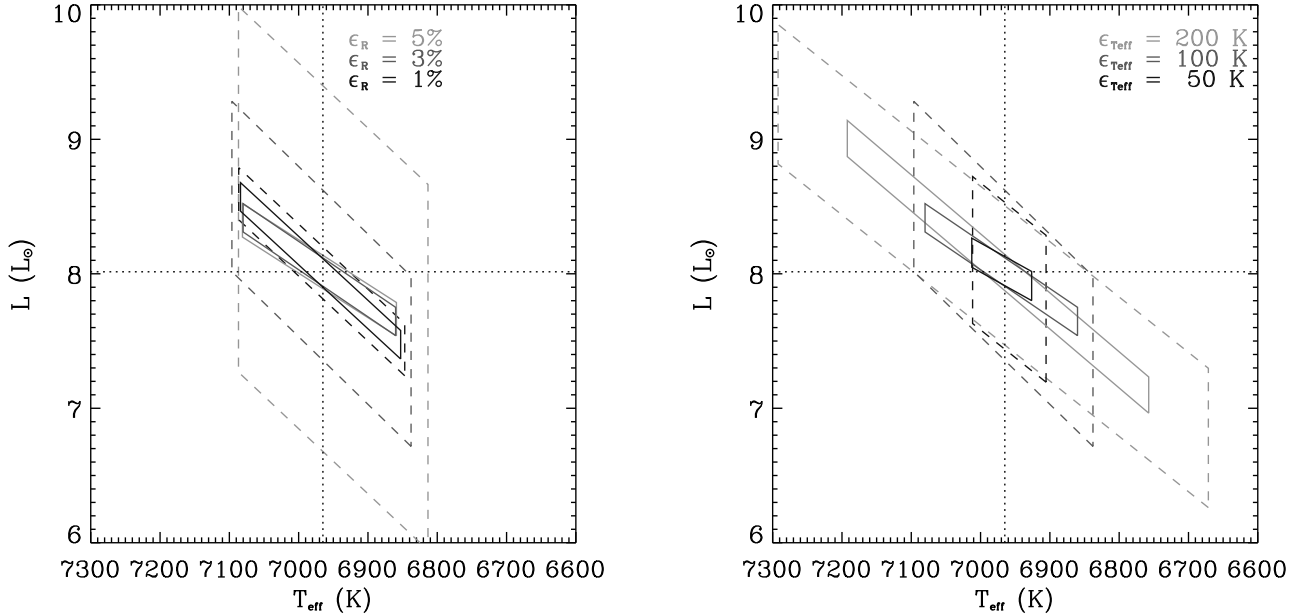


FIG. 9.— The theoretical error boxes for the model parameters of luminosity and effective temperature. The dashed/continuous lines represent the results for the single star (OS_S+AS1)/binary system (OS_{EB}). The left/right panels show the results while reducing the error in observed R/T_{eff} .

We perform simulations to test the effect of recovering the stellar parameters when we identify a mode incorrectly. The model that we test has the true input parameters (\mathbf{P}) that are given in Table 1 with the corresponding model observables (\mathbf{B}) from Table 2. We generate a set of “real observations” (y_i) by adding random errors to the true model observables: $y_i = B_i + \epsilon_i r_i$, where r_i is a random number drawn from a Gaussian distribution with a mean of 0 and standard deviation of 1. To recover \mathbf{P} from y_i , we first make a guess of the solution \mathbf{P}_0 and then use equation (2) to recover the true parameters. We do this for four different scenarios for both the single star and the binary system, without including photometric information ($OS_{S/EB}$ and $OS_{S/EB}+AS1$): (1) using the non-seismic measurements without a mode (black diamonds

in Figure 10, $OS_{S/EB}$), (2) using the non-seismic measurements and a correctly identified mode (red crosses in Figures 10 and 11, $OS_{S/EB}+AS1$), (3) using the non-seismic measurements and an *incorrectly* identified mode — the wrong degree ℓ (blue crosses), and (4) using the non-seismic measurements and an *incorrectly* identified mode — the wrong radial order n (green crosses).

The recovered parameters for 10,000 realizations are shown in Figures 10 and 11. We show only the four parameters of the pulsating star discussed in Section 4.1. The left/right panels show the results for the single star (OS_S/OS_{S+AS1})/binary system ($OS_{EB}/OS_{EB}+AS1$). In each of the panels the black square shows the initial guess of the corresponding parameters, while the dotted lines show the model values from Table 1.

For the single star the left panels of Figure 10 show that the non-seismic observables (OS_S , black diamonds) do not constrain the parameters of the system. Once the mode is included (OS_S+AS1), the solution becomes tightly constrained to a small range of parameter values. When the mode is correctly identified (red crosses) the recovered parameter range is correctly centered on the intersection of the lines. When the mode is incorrectly identified (blue or green crosses) the recovered parameter range is incorrect. It is possible to discard the green solution (the incorrect radial order) because the recovered values of X are outside of the typically accepted values. However, it is not possible to determine if the blue or the red values represent the true input parameters. This means that we are either heavily reliant on obtaining a correctly-labeled mode, or that the formal uncertainties are unrealistic as uncertainties because the systematic error is completely ignored.

For the binary system the right panels of Figure 10 show that the parameter uncertainties agree with those shown in Figure 7; the 1- σ uncertainty is shown by the error-bar. The three solutions with the mode all lead to well-constrained parameter ranges. The solution without the mode (black diamonds) can not be seen very clearly because the values coincide with the red solution, implying that it is the correct identification. The blue and the green solutions can be discarded simply because they are not in agreement with the black solution i.e. there is something incorrect about the mode-identification.

To highlight the inconsistency in the solutions, Figure 11 shows the fitted age for the three solutions including the mode (y-axis) versus the solution without the mode (x-axis). If the mode were correctly identified we would expect the solutions to approximately follow the bisector. This is precisely what we see in both panels. When identifying the mode with an incorrect degree (blue) or the incorrect radial order (green) there is a systematic offset, which implies an incorrectly labeled mode. The difference between the left and the right panels is that we included photometric information in the latter ($OS_{EB}+AS2/AS3$): here the offset is much clearer making it easier to detect the incorrectly-identified mode.

This question can be alternatively posed to ask if we can use the distribution of model solutions to actually identify the oscillation mode. Figure 12 shows a representative sample of the distribution of model solutions of similar simulations for the recovered age parameter. Each of the panels shows the recovered age without including the mode *minus* the recovered age using an arbitrarily-identified mode. We show just the results for the most ambiguous solutions, because all of the other mode identifications led to very clear discrepancies between the two solutions. For the simulations our observations come from a stellar model with a value of convective core overshoot parameter $\alpha_{ov} = 0.3$. We show results when we assume that the inverting model has a value of $\alpha_{ov} = 0.3$ (correct) and 0.0 (incorrect). The top panel shows the results when the mode identification is correct $(\ell, m, n) = (1, -1, 9)$. The middle and lower panels show the results when the mode is labeled incorrectly: $(0, 0, 9)$ and $(1, 0, 9)$. In both panels we can see that even with some errors in our assumptions about the model, we can safely constrain, or even label, the mode with the correct identification from the top panel. This

does not imply that the identified mode is insensitive to α_{ov} , simply that by comparing solutions from the same model any possible systematic error is eliminated.

6. CONCLUSIONS

Seismology of δ Scuti stars has had limited success due to the inability to obtain a unique model of the star and more importantly the difficult task of mode-identification due to rotation, evolution and a deficiency in our understanding of mode-excitation mechanisms. A possible method for overcoming these obstacles, as suggested by many authors, is to study pulsating stars in detached eclipsing spectroscopic binary systems. In this paper we used singular value decomposition (SVD) to quantify the advantages of studying pulsating stars in eclipsing binaries over single field stars, by comparing the parameter uncertainties and the ability to detect an incorrectly-labeled mode in both cases.

We have demonstrated that SVD is a powerful tool to assess the parameter constraints in various systems considering the available measurements. This method assumes that we are relatively close to the parameter solution so that the model derivatives can be described locally as linear. This implies that the results are not extendable to other values where we can no longer extrapolate linearly to estimate observables. We considered the set of parameters shown in Table 1 and deviating much from these values will require new calculations. This work also imposed various assumptions and they must be taken into account. For example, the derivatives are calculated from the ASTEC (Christensen-Dalsgaard 2008) stellar code, and they may vary (hopefully only slightly) from one code to the next.

We have shown that as the measurement errors on the photometric information are varied, the roles of the observables change especially for the single star. In particular, R and $(r-i)$ play similar roles for determining M , and $(i-z)$ and $[M/H]$ for determining Z . The distance d is uniquely determined by π when no photometric information is included, while the colors and magnitude contribute to determining d when these are included, primarily due to the error on the parallax. When no oscillation mode is included, then all of the observables are important for constraining the parameters even poorly, and the inclusion of a correctly identified mode replaces the role of R for determining M .

For the binary system the photometric information does not have as much impact as it does for the single star, partially because these observations are blended values resulting from the two components. However on reaching precisions of ~ 0.003 mag, then the photometric observables begin to dominate the roles of R_A , $T_{eff A}$, $[M/H]$, and T_{BA} for determining the stellar parameters. In particular, $(r-i)_{EB}$ yields similar information to $T_{eff A}$.

For a single star system correctly identifying an oscillation mode is necessary to reduce the parameter uncertainties to values that are useful. On the other hand, a binary system contains enough information, without having to use the identified mode to constrain the stellar parameters well. In fact, including the identified mode does not improve the parameter uncertainties, emphasizing its utility for learning something else about the star. This same trend can be seen for the error box in the H-R

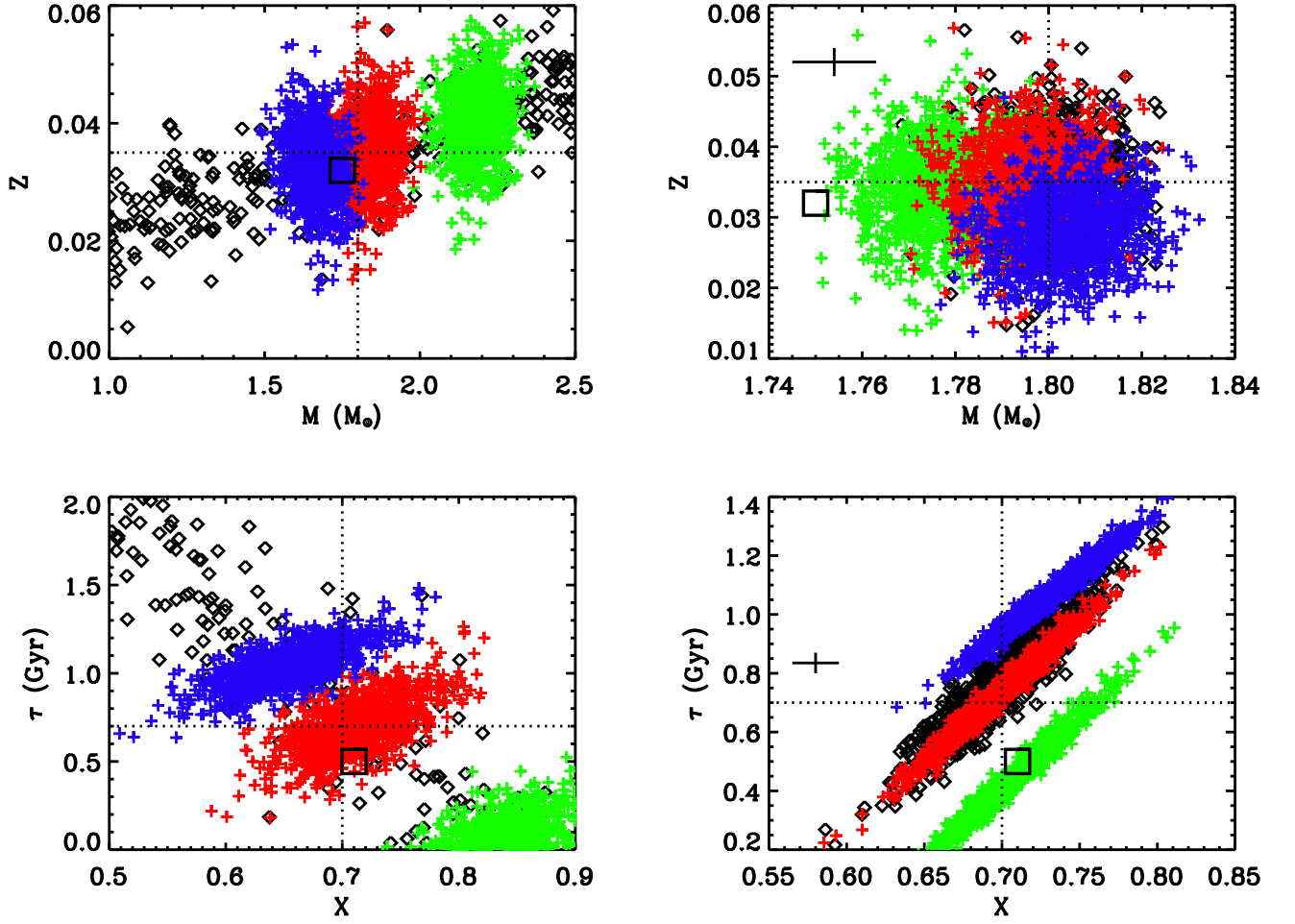


FIG. 10.— Fitted parameters from simulations using OS_{EB} and $OS_{EB}+AS1$. The left/right panels show the results for the single star/binary. The color-code is as follows: black — no mode included; red, green and blue — including a mode, with various identifications: red — correctly identified; blue — incorrectly labeled degree; green — incorrectly labeled radial order. The intersection of the dotted lines are the true values of the input parameters, the black square shows the values of the initial guess, and the error bars on the right panel are the $1-\sigma$ uncertainties for the binary system (see Fig. 7).

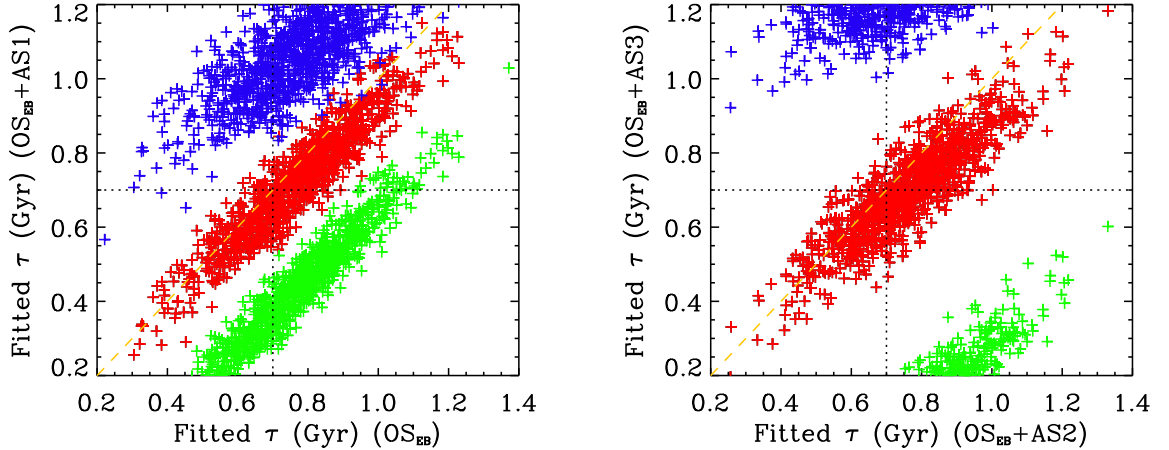


FIG. 11.— Fitted age from the simulations when a mode is (y-axis) and is not (x-axis) included as an observational constraint. The color code is the same as Fig. 10, and the left/right panels show the results for $OS_{EB}+AS1/AS3$.

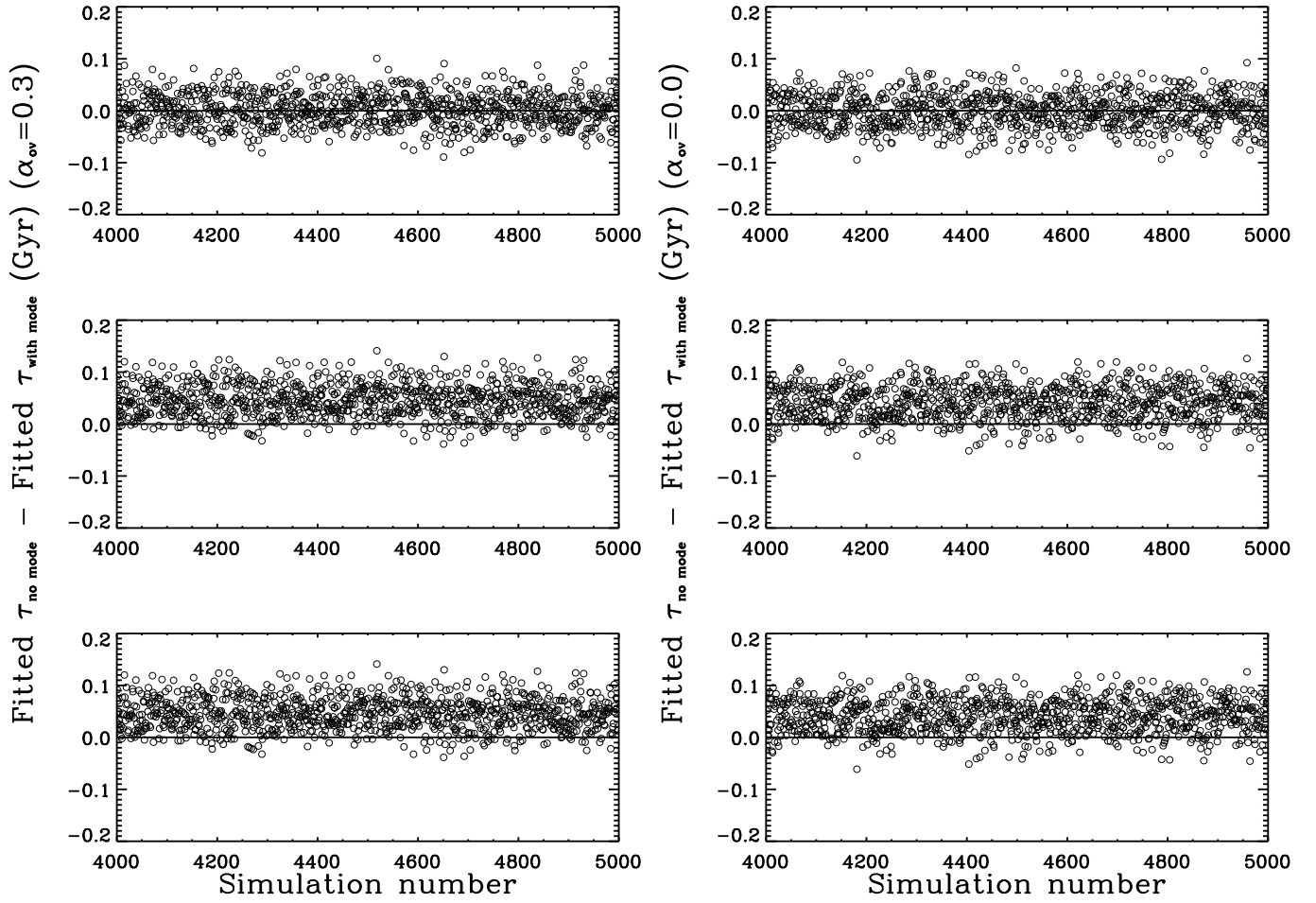


FIG. 12.— Fitted age from simulations using OS+AS2 and OS+AS3. The left/right panels show the results for inversions using the correct/incorrect model ($\alpha_{\text{ov}} = 0.3/0.0$). From top to bottom, the simulations assume a mode identification of $(\ell, m, n) = (1, -1, 9)$ (correct), $(0, 0, 9)$ (incorrect) and $(1, 0, 9)$ (incorrect).

diagram: it does not shrink for the binary system when the mode is included or the errors in R_A are improved. For the single star, however, improving R leads directly to shrinking the error box in the luminosity axis only when a correctly labeled mode is included.

Other parameter values were also considered in this study; we varied the primary mass of the star ($1.80 M_\odot$ and $2.50 M_\odot$), the mass ratio of primary to secondary (1.10 and 1.60), the evolutionary stage of the primary star (central hydrogen mass fraction of 0.50 [MS] and 0.15 [end of MS]), and the metallicity of both stars (0.020 and 0.035). For a single star identifying a mode has more impact on the reference model than the more evolved model and for both the single star and the binary system the higher metallicity model benefited more from the photometric information. However, changing the size of the primary mass did not change the uncertainty dependencies (Creevey 2008).

Because mode-identification in δ Scuti (and other) stars is a complicated task, we addressed whether an incorrectly-labeled mode could be correctly diagnosed using the observational constraints provided by the single star and the detached eclipsing binary system. We used simulations to test the effects of recovering stellar parameters with arbitrarily-identified oscillation modes. We found that for the single star, it is necessary to identify the mode unambiguously, because the recovered solutions using an incorrect or a correct mode identification are not distinguishable. Meanwhile for the binary system, an incorrectly-identified mode can be diagnosed by simply comparing the parameter solutions when the mode is included and not. If the mode is correctly identified, the solutions are in agreement.

Taking this discussion slightly further, in the binary system we also showed that we could in fact tightly con-

strain (and even identify correctly) the pulsation mode parameters by comparing the distribution of model solutions with and without a mode. The model solutions are in agreement when the mode is correctly identified even if the assumptions on the interior physics are slightly incorrect. This type of test and this method of mode-identification has not yet been done with available observational data.

It is clear that studying pulsations in binary systems has its complexities observationally, however, the extra effort is definitely worth it. Apart from the advantage of using the screening effect of the pulsations during eclipse to help identify the mode, this study emphasizes the power that the binary measurements have for determining fundamental parameters and subsequently constraining and even identifying the mode.

In this paper we use the SVD technique to compare the constraints for single stars and binary systems. We note, however, that with the flood of data from space-based missions, this type of study can be subsequently extended to investigate which detached eclipsing binary systems provide the best astrophysical laboratories.

Part of this work was supported by a graduate student *Newkirk Fellowship* at the High Altitude Observatory/National Center for Atmospheric Research, Boulder, CO, USA. This work was also supported by the European Helio- and Asteroseismology Network (HELAS), a major international collaboration funded by the European Commission's Sixth Framework Programme. We thank the referees for comments and suggestions that greatly improved the presentation and the scientific content of the manuscript.

REFERENCES

- Aerts, C., & Harmanec, P. 2004, Spectroscopically and Spatially Resolving the Components of the Close Binary Stars, 318, 325
- Arentoft, T., et al. 2007, A&A, 465, 965
- Baglin, A., Auvergne, M., Catala, C., Michel, E., Goupil, M. J., Samadi, R., Popielsky, B., & The COROT Team 2002, IAU Colloq. 185: Radial and Nonradial Pulsations as Probes of Stellar Physics, 259, 626
- Bahcall, J. N., & Pinsonneault, M. H. 1992, ApJ, 395, L119
- Bakos, G. Á., Lázár, J., Papp, I., Sári, P., & Green, E. M. 2002, PASP, 114, 974
- Balona, L. A. 2000, MNRAS, 319, 606
- Bíró, I. B., & Nuspl, J. 2005, Tidal Evolution and Oscillations in Binary Stars, 333, 221
- Böhm-Vitense, E. 1958, Z. Astrophys., 46, 108
- Borucki, W. J., et al. 2003, Scientific Frontiers in Research on Extrasolar Planets, 294, 427
- Breger, M. 2000, Delta Scuti and Related Stars, 210, 3
- Breger, M., et al. 2005, A&A, 435, 955
- Briquet, M., & Aerts, C. 2003, A&A, 398, 687
- Brown, T. M., Christensen-Dalsgaard, J., Weibel-Mihalas, B., & Gilliland, R. L. 1994, ApJ, 427, 1013
- Brown, T. M., & Charbonneau, D. 2000, Disks, Planetesimals, and Planets, 219, 584
- Bruntt, H., et al. 2010, MNRAS, 405, 1907
- Burke, K. D., & Thompson, M. J. 2006, Proceedings of SOHO 18/GONG 2006/HELAS I, Beyond the Spherical Sun, 624, 107
- Christensen-Dalsgaard, J. 2008, Ap&SS, 316, 13
- Costa, J. E. S., et al. 2007, A&A, 468, 637
- Creevey, O. L., et al. 2005, ApJ, 625, L127
- Creevey, O. L., Brown, T. M., Jiménez-Reyes, S., & Belmonte, J. A. 2006, Astrophysics of Variable Stars, 349, 211
- Creevey, O. L., Monteiro, M. J. P. F. G., Metcalfe, T. S., Brown, T. M., Jiménez-Reyes, S. J., & Belmonte, J. A. 2007, ApJ, 659, 616
- Creevey O. L. 2008, PhD thesis, Universidad de La Laguna, Spain.
- Creevey, O. L., et al. 2009, A&A, 507, 901
- Daszyńska-Daszkiewicz, J., Dziembowski, W. A., Pamyatnykh, A. A., Breger, M., Zima, W., & Houdek, G. 2005, A&A, 438, 653
- Daszyńska-Daszkiewicz, J., Dziembowski, W. A., & Pamyatnykh, A. A. 2007, Acta Astronomica, 57, 11
- Dupret, M.-A., De Ridder, J., De Cat, P., Aerts, C., Scuflaire, R., Noels, A., & Thoul, A. 2003, A&A, 398, 677
- Eggleton, P. P., Faulkner, J., & Flannery, B. P. 1973, A&A, 23, 325
- Escolà-Sirisi, E., Juan-Samsó, J., Vidal-Sáinz, J., Lampens, P., García-Melendo, E., Gómez-Forrellad, J. M., & Wils, P. 2005, A&A, 434, 1063
- Featherstone, N., Browning, M. K., Brun, A. S., & Toomre, J. 2007, BAAS, 38, 117
- Fox Machado, L., Pérez Hernández, F., Suárez, J. C., Michel, E., & Lebreton, Y. 2006, A&A, 446, 611
- Gamarova, A. Y., Mkrtichian, D. E., & Rodríguez, E. 2005, Tidal Evolution and Oscillations in Binary Stars, 333, 258
- Garrido, R. 2000, Delta Scuti and Related Stars, 210, 67
- Gough, D. O., & Thompson, M. J. 1990, MNRAS, 242, 25
- Goupil, M.-J., Dupret, M. A., Samadi, R., Boehm, T., Alecian, E., Suarez, J. C., Lebreton, Y., & Catala, C. 2005, JA&A, 26, 249
- Guzik, J. A., & Bradley, P. A. 1995, Delta Scuti Star Newsletter, 9, 7
- Hadrava, P. 1995, A&AS, 114, 393
- Hadrava, P. 2009, A&A, 494, 399
- Handler, G. 2002, Observational Aspects of Pulsating B- and A Stars, 256, 71

- Hekker, S., et al. 2010, *ApJ*, 713, L187
- Henry, G. W. 1998, *Technical Advances in Aeronautics, Space Sciences and Technology, Earth Systems Sciences, Global Hydrology, and Education*, 2, 679
- Hilditch, R. W., Howarth, I. D., & Harries, T. J. 2005, *MNRAS*, 357, 304
- Horner, S. D., Kennelly, E. J., Brown, T. M., Noyes, R. W., Korzennik, S. G., Nisenson, P., Yang, S., & Walker, A. R. 1996, *BAAS*, 28, 916
- Iglesias, C. A., & Rogers, F. J. 1996, *ApJ*, 464, 943
- Kennelly, E. J., Walker, G. A. H., & Matthews, J. M. 1990, *Confrontation Between Stellar Pulsation and Evolution*, 11, 320
- Kirbiyik, H., Civelek, R., & Kiziloğlu, N. 2005, *Ap&SS*, 295, 473
- Koch, R. H. 1960, *AJ*, 65, 374
- Lampens, P., & Boffin, H. M. J. 2000, *Delta Scuti and Related Stars*, 210, 309
- Lastennet, E., Valls-Gabaud, D., & Oblak, E. 2000, *IAU Symposium*, 200, 164P
- Lejeune, T., Cuisinier, F., & Buser, R. 1997, *A&AS*, 125, 229
- Maceroni, C. 2006, *Astrophysics of Variable Stars*, 349, 41
- Maceroni, C., Cardini, D., Damiani, C., Gandolfi, D., Debosscher, J., Hatzes, A., Guenther, E. W., & Aerts, C. 2010, *arXiv:1004.1525*
- MacGregor, K. B., Jackson, S., Skumanich, A., & Metcalfe, T. S. 2007, *ApJ*, 663, 560
- Matthews, J. M. 2004, *Bulletin of the American Astronomical Society*, 36, 1563
- Metcalfe, T. S., Creevey, O. L., & Christensen-Dalsgaard, J. 2009, *ApJ*, 699, 373
- Metcalfe, T. S. et al. 2010, *ApJ*, 723, 1583
- Miglio, A., & Montalbán, J. 2005, *A&A*, 441, 615
- Pamyatnykh, A. A., Dziembowski, W. A., Handler, G., & Pikall, H. 1998, *A&A*, 333, 141
- Pollacco, D., et al. 2006, *Ap&SS*, 304, 253
- Press, W. H., Teukolsky, S. A., Vetterling, W. T., & Flannery, B. P. 1992, *Numerical Recipes in Fortran*, (2nd ed.; Cambridge University Press; 670)
- Ribas, I., Jordi, C., & Torra, J. 1999, *MNRAS*, 309, 199
- Ribas, I., Fitzpatrick, E. L., Maloney, F. P., Guinan, E. F., & Udalski, A. 2002, *ApJ*, 574, 771
- Saesen, S., et al. 2010, *A&A*, 515, A16
- Semeniuk, I. 2001, *Acta Ast.*, 51, 75
- Sousa, S. G., Santos, N. C., Israelian, G., Mayor, M., & Monteiro, M. J. P. F. G. 2006, *A&A*, 458, 873
- Southworth, J., Smalley, B., Maxted, P. F. L., & Etzel, P. B. 2004, *The A-Star Puzzle*, 224, 548
- Stello, D., et al. 2010, *ApJ*, 713, L182
- Talamantes, A., Sandquist, E. L., Clem, J. L., Robb, R. M., Balam, D. D., & Shetrone, M. 2010, *AJ*, 140, 1268
- Templeton, M., Basu, S., & Demarque, P. 2001, *ApJ*, 563, 999
- Viskum, M., Kjeldsen, H., Bedding, T. R., dall, T. H., Baldry, I. K., Bruntt, H., & Frandsen, S. 1998, *A&A*, 335, 549
- York, D. G., et al. 2000, *AJ*, 120, 1579
- Zima, W. 2006, *A&A*, 455, 227
- Zima, W., et al. 2006, *A&A*, 455, 235